Mechanobiology in Medicine 3 (2025) 100099

Contents lists available at ScienceDirect

Mechanobiology in Medicine

journal homepage: www.sciencedirect.com/journal/mechanobiology-in-medicine

Full Length Article

# Mechanotransductive N-cadherin binding induces differentiation in human neural stem cells

McKay Cavanaugh [a], Rebecca Kuntz Willits [a,b,*]

[a] Department of Bioengineering, Northeastern University, Boston, MA, USA
[b] Department of Chemical Engineering, Northeastern University, Boston MA, USA

ARTICLE INFO

*Keywords:*
N-Cadherin
Homophilic mechanotransduction
Stem cell
Differentiation

ABSTRACT

The neural stem cell niche is a complex microenvironment that includes cellular factors, secreted factors, and physical factors that impact stem cell behavior and development. Cellular interactions through cadherins, cell–cell binding proteins, have implications in embryonic development and mesenchymal stem cell differentiation. However, little is known about the influence of cadherins within the neural stem cell microenvironment and their effect on human stem cell maintenance and differentiation. Therefore, the purpose of this study was to develop synthetic substrates to examine the effect of cadherin mechanotransduction on human neural stem cells. Glass substrates were fabricated using silane, protein A, and recombinant N-cadherin; we used these substrates to examine the effect of N-cadherin binding on neural stem cell proliferation, cytoskeletal structure and morphology, Yes-associated protein-1 (YAP) translocation, and differentiation. Bound exogenous N-cadherin induced concentration-dependent increases in adherens junction formation, YAP translocation, and early expression of neurogenic differentiation markers. Strong F-actin ring structures were initiated by homophilic N-cadherin binding, eliciting neuronal differentiation of cells within 96 h without added soluble differentiation factors. Our findings show that active N-cadherin binding plays an important role for differentiation of human iPS-derived neural stem cells towards neurons, providing a new tool to differentiate cells *in vitro*.

## 1. Introduction

Neural stem cells (NSCs) have the capacity for self-renewal and differentiation; they are one of the only sources of new neuronal, astrocytic, and glial cells in human adults. NSCs (also called type B cells) are found to reside in two main regions of the brain, the subventricular zone along the lateral ventricle and the subgranular zone in the dentate gyrus of the hippocampus[1] providing new olfactory neurons and hippocampal neurons respectively.[2,3] The subventricular zone niche of NSCs is a highly complex microenvironment, comprised of many different factors that contribute to NSC fate, including extracellular matrix (ECM) components, cellular components, transient cells, and other constituents. Understanding how individual components of the niche direct cell differentiation could be a powerful therapeutic to treat neurodegeneration. In this regard, the focus of this work is on cell–cell binding, which allows for structural integrity of the niche and coordination between different cell types for maintenance and differentiation.

One important cell surface ligand used for cell–cell communication is cadherin. N-cadherin, discovered in neural cells, and E-cadherin, discovered in epithelial cells, are two classical cadherin subtypes typically found within the subventricular zone. Cadherins sense, transduce, and deliver biochemical outcomes from mechanical stimuli.[4–6] They are calcium dependent transmembrane glycoproteins[7] with 5 extracellular repeat domains. At cell–cell contact points, forces from surrounding cells are transduced intracellularly and produce a downstream intracellular cascade in a complex and dynamic nature that includes binding, clustering, stabilization of junctional components and reorganization of cytoskeletal architecture with potential interactions with the nucleus.[8,9] These forces, termed mechanotransduction, are a dynamic signaling process[8] with several pathways that work concomitantly with it including intracellular cytoskeletal rearrangement[10,11] and Yes-associated protein 1 (YAP) signaling.[12–14]

While little is known about the role of N-cadherin mechanotransduction in defining the neural stem cell niche, it has been examined in other settings, such as embryonic development, cancer metastasis, and chondrogenesis of mesenchymal stem cells. N-cadherin binding has been shown to impact neural differentiation of neural stem cells.[15,16] However, the results vary widely and the link to mechanotransduction

* Corresponding author. Department of Chemical Engineering, Northeastern University, Boston, MA, USA
*E-mail address:* r.willits@northeastern.edu (R.K. Willits).

https://doi.org/10.1016/j.mbm.2024.100099
Received 16 August 2024; Received in revised form 30 September 2024; Accepted 9 October 2024
Available online 16 October 2024

through N-cadherin for NSCs is less clear. Therefore, the purpose of this study was to examine the effect of N-cadherin mechanotransduction on human induced pluripotent stem cell derived NSC fate. Glass substrates were functionalized with N-cadherin at various concentrations and cells were examined for their ability to adhere to the substrates. Once confirmed, cultured NSCs were examined for morphology, mechanotransduction, and differentiation status. As directing stem cell fate can provide therapeutic and targeted solutions to deterioration in the brain, a better understanding of the contributions and roles of each component can enable the design of more effective tissue engineered solutions to combat neurodegeneration.

## 2. Materials and methods

### 2.1. Materials

Human induced pluripotent stem cell-derived neural stem cells (hNSCs) were purchased from Alstem cat #: hNSC1; Richmond, CA. Recombinant human epidermal growth factor (EGF, cat# AF-100-15) and recombinant human fibroblast growth factor (FGF, cat# 100-18 B) were purchased from PeproTech; Cranbury, NJ. The following products were purchased from Sigma (St. Louis, MO): donkey serum (DK) (cat#: S30-100 mL), Hanks' Balanced Salts solution (HBSS with $Mg^{2+}$ and $Ca^{2+}$) (cat#: H1387), Hanks Balanced Salt solution (without $Mg^{2+}$ and $Ca^{2+}$) (HBSS, cat#: H4891), and dimethyl sulfoxide (sterile and ≥99.7 %) (Cat#: D2650). The following items were purchased from VWR (Radnor, PA): DMEM F12, Corning® 10 L DMEM (Dulbecco's Modification of Eagle Medium)/Hams F-12 50:50 Mix (DMEM:F12), powder [-] sodium bicarbonate, L-glutamine (Coring 90-091-pb, cat#: 45,000-536), sodium azide (cat#: 97,064-646), ethylenediamine tetraacetic acid (EDTA) (cat#: BDH9232-500G), and bicinchoninic acid (BCA) assay (Pierce Biotechnology; cat#:PI23225). The following products were purchased from ThermoFisher (Waltham, MA): Gibco™ StemPro™ Neural Supplement (cat#: A1050801), Gibco™ Geltrex™ LDEV-Free, hESC-Qualified, Reduced Growth Factor Basement Membrane Matrix (cat#: A1413302); Corning™ Matrigel™ GFR Membrane Matrix (at# CB40230A), Corning™ glutaGRO Supplement (Corning™ 25015CI), Accutase (cat#: 104–500 mL), RIPA buffer (cat#: 89,901), HALT protease inhibitor cocktail (100*X*) (product#: 1861278) and 0.5 M EDTA solution (product #: 1861275), paraformaldehyde (PFA; cat#: O4042-500), bovine serum albumin (cat#: BP9706100), ethidium homodimer-1 (Invitrogen; cat#: L3224), saponin (Alfa Aesar; cat#: A18820-14), sodium borohydride (MP Biomedical; cat#: 102,894), Hoechst 33,342 (Invitrogen; cat#: H1399), UltraComp ebeads Plus (Invitrogen; cat: 01-3333-41), MitoTracker™ Orange CM-H2TMRos (Invitrogen; cat#: M7511), Molecular Probes™ CyQUANT™ Cell Proliferation Assay (Molecular Probes™ C7026), LIVE/DEAD Viability assay containing calcein-AM and ethidium homodimer-1 (cat#: L3224), Mitotracker (Invitrogen; cat#: M7511), Alexa Fluor 647 Phalloidin (Invitrogen; cat#: A22287), Tris Base (cat#: BP152-500), and PierceTM IgG Elution Buffer (cat#: 21,004). Fluoro-Gel Mounting Medium with Tris Buffer (cat# 17,985-10) was purchased from Electron Microscopy Sciences (Hatfield, PA). Human N-cadherin ELISA kit containing all reagents was purchased from Abcam (Waltham, MA) (cat#: ab254512). All antibodies used, corresponding secondaries and respective manufacturer and concentration used are detailed in Table S1.

The following materials were purchased from ThermoFisher (Waltham, MA): borosilicate coverslips (cat#:12-545-100 P) (3-mercaptopropyl) trimethoxysilane (3-MPTS) (cat#: AAB2372614), 200 proof ethanol (Decon Laboratories; cat#:2701G), sulfo-SMCC (sulfosuccinimidyl 4-(N-maleimidomethyl)cyclohexane-1-carboxylate) (cat#: PI22322), and BupH Phosphate Buffered Saline (BuPBS) (cat#: PI28372). Toluene (cat#: TX0735-5) and Protein A (cat#: P603) were purchased from Sigma (St. Louis, MO). Human recombinant Fc-tagged N-cadherin was purchased from R and D (Minneapolis, MN) (cat#:1388-NC-050) and E-cadherin was purchased from Sino biological (Chesterbrook, PA) (cat# 10,204-H02H).

### 2.2. Substrate preparation

All procedures were performed at room temperature unless otherwise defined. Borosilicate glass coverslips were functionalized with recombinant human N- and E-cadherin proteins; control substrates were adsorbed with Matrigel®. In brief, coverslips (Ø18mm) were cleaned via 5 min sonication in acetone, dried via compressed air, and then cleaned via plasma cleaner for 3 min. Following cleaning, surfaces were silanized via 3-MPTS (5 % v/v) in toluene for 1.5 h. Samples were washed in toluene, ethanol:toluene (1:1), and ethanol. Next, sulfo-SMCC was diluted in Type 1 water with 5 mM EDTA was placed on the sample (0.086 μmol/$cm^2$) for 30 min. Protein A was diluted in BuPBS to be 0.2 mg/mL (0.374 nmol/$cm^2$) and incubated with each surface for 30 min. Following incubation, the surfaces were washed with BuPBS. Lastly, human recombinant Fc-tagged N- or E-cadherin recombinant protein was diluted in Type 1 water and incubated on the substrates for 1 h (Fig. 1A). Following incubation, the surfaces were washed and sterilized by dipping the surfaces in sterile BuPBS, sterile Type 1 water, and sterile 70 % ethanol three times.

Surfaces were analyzed via attenuated total reflection FTIR with a Vertex 70 IR spectrometer following each step of the functionalization process (n = 3). In addition, quantification of the binding of Protein A to the substrate was performed by XPS. Coverslips were fabricated as described above and washed with Type 1 water, let dry and put under vacuum until XPS analysis. A survey was performed on a 400 μm spot from −10 eV to 1350 eV at a 1 eV step size, with 5 scans and 10 ms dwell time. For elements, the following settings were used: carbon binding energy center, 285 eV, width, 20 eV; nitrogen binding energy center, 401 eV, width, 18 eV; oxygen binding energy center, 535 eV, width, 20 eV. The energy step size was 0.1 and pass energy was 50 eV, with 10 scans and 25 ms dwell time. Elemental surveys from each surface were analyzed to find the existence of atoms of interest and average N/C ratio.

### 2.3. Cadherin-bound substrates

Four different applied concentrations (6.68 pmol/$cm^2$, 11.6 pmol/$cm^2$, 20.0 pmol/$cm^2$, and 32.0 pmol/$cm^2$) of N-cadherin substrates were prepared. The amount of N-cadherin applied to the samples was determined by considering the theoretical packing of protein A molecules using a circular estimation with molecular size[17] and then calculated the upper concentration using the binding ability of protein A with up to 5 Fc (N-cadherin) molecules and the lower concentration was determined by estimating a 1:1 protein A:N-cadherin. Therefore, incremental increases in the amount of applied cadherin were included to examine cell response and determine a relevant range for further testing.

To determine the amount of cadherin on the substrates, cadherin was eluted using an acidic elution buffer known to break the interaction between the Fc and protein A molecules. Elution buffer (pH 2.8) and neutralizing 1.0 M Tris buffer (pH 8.8) were brought to room temperature. Then, 1 mL of the elution buffer was washed over the cadherin-bound surfaces and added to a 1.5 mL microcentrifuge tubes with 100 μL of the neutralizing buffer. The solutions were then placed in the −80 °C freezer for quantification via ELISA.

A SimpleStep ELISA® designed to target human N-cadherin was used according to manufacturer's directions. Standards of 0.045 pmol/ml, 0.022 pmol/ml, 0.0056 pmol/ml, and 0 pmol/ml were created using the same recombinant N-cadherin and acid elution buffer used on substrates. Using the standard curve, the amount of eluted N-cadherin was calculated.

### 2.4. Cell expansion and maintenance

Human induced pluripotent stem cell-derived neural stem cells (hNSCs) were purchased as the neural stem cells. Cells were cultured (37 °C and 5 % $CO_2$) with maintenance media. Maintenance media is

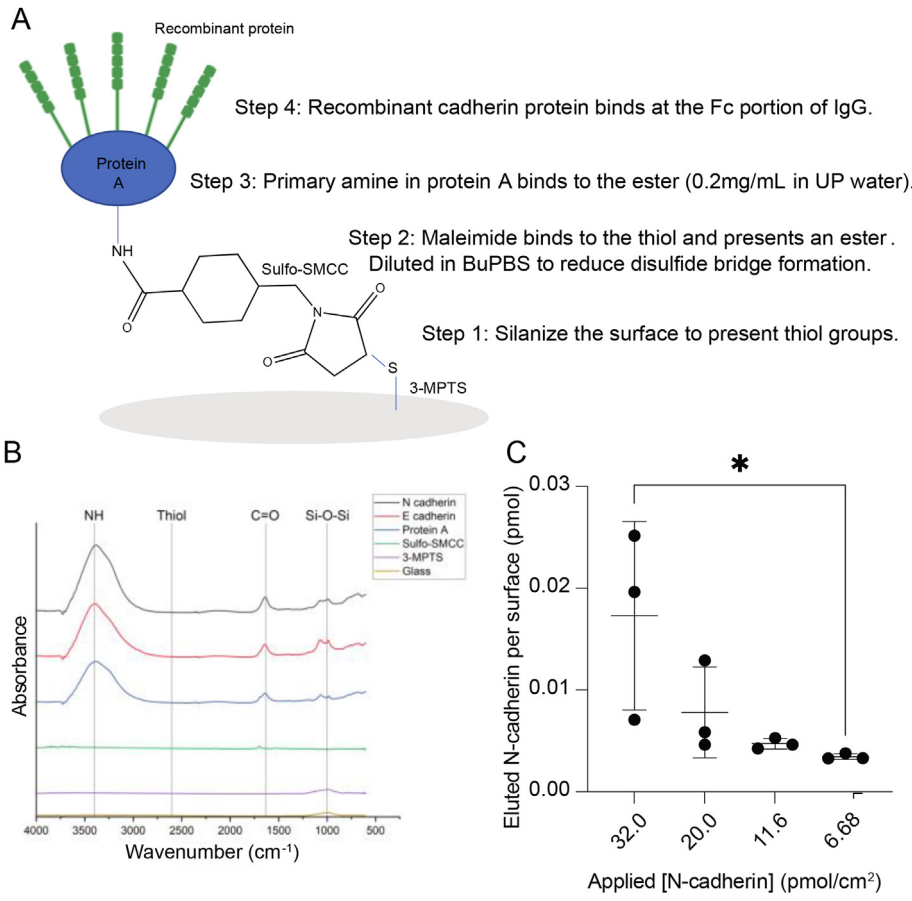


**Fig. 1.** A. Schematic of 4 step process for recombinant cadherin tethering on 2D glass. B. FTIR analysis following each subsequent surface fabrication step. C. Quantification of eluted N-cadherin from surfaces via ELISA. Significantly less N-cadherin was eluted from N-Cad 1 surfaces (3.5 fmol) compared to N-Cad 5 (17 fmol) substrates.

composed of DMEM:F12, 20 ng/mL EGF, 20 ng/mL FGF, 1*X* StemPro™ Neural Supplement and 2 mM glutaGRO. Media was changed every other day. Matrigel® or Geltrex® was used to coat flasks for expansion of cells prior to use on functionalized surfaces at a concentration of 1:50 diluted in DMEM:F12 as described by manufacturer. Cells were passaged at approximately 90 % confluency. To passage, cells were lifted via Accutase and seeded at a density of 10,000 cells/cm$^2$. Prior to experiments, potency of hNSCs was verified via flow cytometry (detailed below) to show nestin expression. Cells were deemed multipotent if the nestin positive cell population was above 95 %. Cells were used between passages 2 and 8.

### 2.5. Cell studies

Substrates were pre-wet with DMEM:F12 prior to cell seeding for at least 30 min. To study the interaction of cells with tethered cadherin, individual cells were required. Cells were seeded at 10,000 cells/cm$^2$. Duration of each experiment is noted below.

*Cadherin expression:* To determine baseline cadherin expression of hNSCs, protein was isolated from cells after reaching confluency under growth conditions on Matrigel at 96 h. Briefly, cells were washed with HBSS and lifted via Accutase from the substrates. Cells were washed twice with cold HBSS via centrifugation at 300×*g* for 5 min at 4 °C. The cell pellet was resuspended in RIPA buffer with HALT protease inhibitor cocktail and 5 mM EDTA following the manufacturer recommendations. The samples were sonicated for 30 s and then placed on ice and shaken gently for 15 min. Next, the solution was centrifuged at 14,000×*g* for 15 min at 4 °C to collect the cellular debris. The resulting supernatant, containing the extracted protein, was then collected. A BCA assay was used to quantify total protein concentration using a standard curve from 0 to 2 mg/mL of bovine serum albumin. Capillary electrophoresis (Jess Protein Simple) was used to quantify relative amounts of the protein of interest as detailed in our previous publication.[18] Each well was loaded with the primary antibody of interest and the reference protein β-actin. Rabbit secondary HRP-conjugated antibodies were loaded, the plate was centrifuged, and the samples were run in the Jess. Peak area for each antibody was analyzed via the Compass for SW software by normalizing the area under the peak for each protein of interest to the reference protein in each capillary to calculate the relative amount of each protein.

*Cell viability:* Cell viability was assessed at 60 h post-seeding on both N and E-cadherin surfaces. Cells were washed 3 times with HBSS. Following the manufacturer's protocol, 5 μL of calcein AM and 20 μL of ethidium homodimer were mixed in 10 mL HBSS. Samples were incubated with the solution for 30 min protected from light. Samples were then imaged via fluorescence to visualize viability. No viable cells were found on E-cadherin surfaces therefore, further work was completed using N-cadherin surfaces only.

*Cell adhesion:* Cell adhesion was assessed at 4 h post seeding on N-cadherin surfaces. Surfaces were washed with HBSS to remove any non-adherent cells. Cells were lifted via Accutase and pelleted. The pellet was washed with HBSS twice and lysed via freeze/thaw at −80 °C. Approximate cell count was determined via CyQuant assay by following the manufacturer's protocol and a standard curve ranging from 0 to 50,000 cells. At least n = 3 samples were used for each concentration group; Matrigel® surfaces were used as a positive control and protein A surfaces was used as a negative control.

*Cell proliferation*: Cell proliferation was quantified at 72 h of culture by CyQuant. Approximate cell count was determined via CyQuant assay by following the manufacturer's protocol and a standard curve ranging from 20,000 to 200,000 cells. Doubling time was calculated for each substrate using the average number of cells found during adhesion studies. In addition, Ki67 and SOX2 labeling were examined at 24 h.

*Cell morphology and mechanotransduction (YAP):* To examine the cell morphology and YAP, cells were cultured for 24 h and prepared for ICC.

*Cell differentiation*: For differentiation studies, cells were seeded at approximately double the seeding density and were cultured for 96 h and prepared for ICC or for flow cytometry.

### 2.6. Immunocytochemistry (ICC) preparation

*Fixation and permeabilization:* Samples were fixed with freshly made 4 % PFA in HBSS for 10 min and the samples were washed with HBSS 3*x* for 5 min each on a rocker. The cells were permeabilized with 0.5 % saponin for 15 min. The cells were washed twice with 1 mg/mL sodium borohydride for 10 min. Next, the cells were washed with HBSS 3*x* for 5 min.

*ICC for N and E-cadherin:* Samples were blocked to minimize nonspecific binding with 5 % donkey serum in 0.1 % saponin for 60 min and then washed with HBSS 3*x* for 5 min each. Next, the primary antibodies were diluted in 0.1 % saponin and incubated on samples at 4 °C overnight on a rocker. The antibody solution was removed and the samples were washed 3*x* for 5 min with HBSS. Secondary antibodies were diluted in 0.1 % saponin. Cells were incubated with secondary antibodies overnight at 4 °C and then washed with HBSS 3*x* for 5 min each. Lastly, nuclear label Hoechst 33,342 (1:200 in PBS) was incubated with the samples for 1 h. Samples were mounted using Fluoro-Gel Mounting Medium and imaged on a Zeiss AxioObserver, an inverted fluorescent microscope, at 63*X*.

*ICC for other proteins:* Samples were blocked with 7.5 % BSA in 0.1 % saponin for 60 min to reduce background. The cells were then washed with HBSS 3 times for 5 min each. Next, the primary antibodies were diluted in the block solution and incubated with samples at 4 °C overnight. The antibody solution was removed, and the samples were washed 3*x* for 5 min. Secondary antibodies were diluted at 1:400 in the blocking solution. Cells were incubated with secondary antibodies and nuclear stain Hoechst (1:500) for 2 h. For morphology, an extra step was added following secondary antibody staining where phalloidin (1:400) was incubated with the samples for 60 min. Samples were then washed with HBSS 3*x* for 5 min, mounted, and imaged on a Zeiss Observer.

### 2.7. Image analysis

At least 40 individual cells were imaged for each sample (3 replicates; 120 cells per surface type). Samples were excluded if the background had too much debris that interfered with analysis and/or if the cells were touching. Following exclusion, at least 28 cells were analyzed per sample. Representative images are from the 3rd quartile of quantification for morphology, YAP, and differentiation.

*Cell morphology:* ImageJ was used to overlay the F-actin and β-catenin images, the perimeter of the cells was traced, and the area was collected. Nuclear area was determined by taking the Hoechst image, tracing the nuclear shape, and quantifying the area. Cellular protrusions were examined to measure the number of polls on each cell. ImageJ was used to collect the major and minor axis of the cells from the original area outline and the aspect ratio was found by taking the ratio of the major axis to the minor axis; an aspect ratio of 1 is indicative of a circular shape. β-catenin punctates were manually counted by examining the β-catenin images of individual cells; the localization of β-catenin staining was visualized and quantified as diffuse staining or at the edge of the cell membrane. The F-actin and β-catenin images were overlayed via FIJI(ImageJ)[19] and colocalization of the two signals at the actin structures was examined by observing a corresponding signal in the β-catenin image.

*YAP:* ImageJ was used to analyze the intensity of YAP and its location in the cells on the surfaces. Surfaces of N-cad 5 were not utilized due to the lack of significant differences between the N-cad 3 group and N-cad 5 group in previous findings. The Hoechst-labeled nuclei were outlined and used to measure the average intensity of YAP in the nucleus. Then the F-actin image was used to create the outline of the cytoplasm and the average intensity of YAP in the cytoplasm was collected, excluding the nucleus. The ratio of average nuclear YAP intensity and average cytoplasmic YAP intensity was then used to examine translocation of YAP to the nucleus.

*F-actin:* Unique F-actin structures were found in some of the images. To quantify, the area of the F-actin structures was traced around the exterior of the densely clustered F-actin stress fibers; the interior of the structure was also traced. The area was found by subtracting the inside area from the exterior area. Within these structures, the colocalization of YAP and the F-actin structures was quantified by overlaying the two images and assessing the presence of both proteins. The percentage of cells with colocalized YAP:F-actin were then counted for each surface.

*Pluripotency:* Labeling of SOX2 was found within the nuclei; SOX2 positive cells, colocalized with the nuclei image, were then counted and the percent of the total cells was calculated. Ki67 positive cells showed distinct punctates within the nuclei of cells, was used as a marker of dividing cells. Nuclei and Ki67 were overlayed and cells with Ki67 punctates were counted; the percent of cells with Ki67 positive cells was then calculated from the total number of cells within the sample. At least 30 cells per sample were analyzed. The sum of the cells from each image was used to make the total number of cells per each sample. A minimum of 5 images were taken per sample, these images were then quantified via ImageJ.

Determining Cell Fate: Labeling for glial fibrillary acidic protein (GFAP) and nestin, was used to determine that NSCs expressed proteins of type B cells that arise from the SVZ indicating their maintenance as NSCs.[20] To determine if cells had differentiated to neuronal or glial fates β-III tubulin[21] and S100β[22] were used respectively.

### 2.8. Flow cytometry

Flow cytometry was used to quantify the percent of cells within the population that had particular protein expression. Cells were removed from the substrates, centrifuged at 300×*g* for 5 min at 4 °C, and the supernatant was removed. The cells were washed with 100 μL of buffer (0.1 % saponin, 1 % BSA, 2 mM EDTA, and 0.1 % sodium azide in HBSS) and centrifuged at 300×*g* for 5 min at 4 °C. Next, cells were incubated with the primary antibody diluted in flow buffer for 30 min on a rocker, following which the antibody solution was removed via centrifugation at 300×*g* for 5 min at 4 °C. The cells were washed with 100 μL of buffer and the buffer was aspirated following centrifugation. Secondary antibodies were then incubated with the sample for 30 min on a rocker. Cells were then centrifuged, the antibody solution was removed, the cells were resuspended in buffer, and centrifuged at 300×*g* for 5 min at 4 °C. Lastly, cells were resuspended in 200 μL of flow buffer. Isotype controls were used to examine nonspecific binding and to gate positive and negative populations. Cells were analyzed following staining on a Beckman Coulter Cytoflex S. UltraComp ebeads Plus were used for compensation following the manufacturer's protocol for β-III tubulin and S100β as these were not uniformly expressed in the cell populations tested. At least 30,000 events were collected per sample. Data was analyzed to see the percent expression protein markers of cell population expression using CytExpert for multicolor flow and FlowJo was used to determine differences between isotype controls and stained populations in single stained samples.

### 2.9. Statistical analysis

To examine the effect of cadherin mechanotransduction on hNSCs, data was tested for normality and homogeneity of variance to meet the

assumptions for the general linear model (GLM). The residuals were examined to see if they were heteroscedastic and Gaussian, fitting the assumption of the GLM was tested by Brown-Forsythe or Bartlett's test (heteroscedasticity) and D'Agostino, Anderson-Darlin, Shapiro–Wilk and Kolmogorov–Smirnov tests (Gaussian residuals). Comparisons between two groups were tested using a student's t-test (cadherin protein expression and doubling time). For comparisons between more than two groups, a one-way ANOVA was used with a Bonferroni *post hoc* comparison test. If the assumptions of GLM were not met, a nonparametric Kruskal–Wallis test with Dunn's multiple comparison *post hoc* test was used to show differences between groups (applied N-cadherin concentration, cell adhesion, area, aspect ratio, number of β-catenin punctates, and SOX2 expression). A significance value of $p = 0.05$ to was used to show differences between groups with at least $n = 3$ independent samples per group. For all image analysis each sample was the average of at least 28 cells. As detailed in the image analysis portion, data is displayed as individual data points with mean and ± standard deviation. Asterisks on graphs indicate p = value (<0.05 (*), <0.0021 (**), <0.00021 (***), and <0.0001 (****)).

## 3. Results

The hNSCs used in this report were purchased cells; nestin expression via flow cytometry was used to show continued multipotency prior to use in any experiments. Fig. S1 displays representative flow cytometry analysis where at least 95 % of cells expressed nestin when compared to the isotype control.

### 3.1. Substrate characterization

Recombinant cadherins were tethered to glass surfaces shown in schematic Fig. 1A. FTIR after each subsequent addition shows respective peaks following addition of layers leading to protein functionalized glass slides. Clean glass has the Si–O–Si peak at approximately 1000, thiol present after silanization in a weak peak at 2550, peak for ester group present approximately 1210–1163 and broad peaks characteristic of an amine from 2500 to 3800 for protein A layers and recombinant cadherin. The presence of tethered recombinant cadherin was visualized via FTIR as shown in Fig. 1B. The amount of Protein A bound to the surface was evaluated using XPS (Fig. S2), where a complete coverage of silane + Sulfo-SMCC + Protein A would lead to N/C ratio of 745/2433. The N/C ratio was calculated to be 0.168, or 150 +/− 6.9 pmol/cm$^2$, equivalent to ~36 % coverage of a monolayer of silanes.[23,24]

Eluted N-cadherin was quantified with ELISA (Fig. 1C) and showed an increase in the amount of N-cadherin quantified as applied cadherin increased. The amount of cadherin eluted from the 6.68 pmol/cm$^2$ concentration surfaces was 3.5 fmol ± 0.28 fmol, the amount eluted from 11.6 pmol/cm$^2$ surfaces was 4.7 fmol ± 0.51 fmol, the amount eluted from 20.0 pmol/cm$^2$ surfaces was 7.8 fmol ± 4.5 fmol, and the amount eluted from 32.0 pmol/cm$^2$ surfaces was 17 fmol ± 9.3 fmol. In all cases, the percentage bound was only approximately 0.02 % of what was applied. The lowest concentration surface had significantly less cadherin eluted compared to the highest cadherin surfaces. For simplicity, the sample groups will be described as follows: N-cad 1 (3.5 fmol), N-cad 2 (4.7 fmol), N-cad 3 (7.8 fmol), and N-cad 5 (17 fmol).

### 3.2. Cellular characterization

*Cadherin expression and cell viability:* N and E-cadherin protein expression in the NSCs was quantified by capillary electrophoresis; this protein analysis high levels of N-cadherin expression with very little E-cadherin expression (Fig. 2A). NSCs seeded onto the cadherin modified substrates only survived when N-cadherin was present (Fig. 2B). In summary, the hNSCs in this study expressed N-cadherin, and not E-cadherin, and for cell viability, cadherin-binding is homophilic.

*Cell adhesion and proliferation*: Both cell adhesion and proliferation were quantified via CyQuant assay. Adhesion was determined at 4 h post seeding. No cells adhered to the negative control of protein A (0 cells ± 0). Adhesion on N-cad 1 surfaces did not differ significantly from the negative control (2830 cells ± 2170 cells), as well as on the N-cad 2 (10,200 cells ± 3760 cells) concentration surfaces. However, adhesion significantly increased on N-cad 3, N-cad 5, and the positive control (Matrigel®) (23,600 cells ± 10,200 cells, 22,300 cells ±3320 cells, and 29,500 cells ± 15,300 cells respectively) compared to the negative control (Fig. 3A). Cell doubling time ($d_t$) was quantified to assess proliferation after 72 h in culture (Fig. 3B) using $d_t = \frac{\ln(2)}{g}$ where $g = \frac{ln\left(\frac{N(t)}{N(0)}\right)}{t}$ and N(t) was the number of cells via Cyquant at the time of assay and N (0) was the average number of cells via Cyquant that adhered (at 4 h); no significant differences were found in doubling times.

*Cell morphology:* The effect of exogenous N-cadherin substrates on cell size was examined via essential components of adherens junctions that anchor cadherins at the membrane, including N-cadherin (magenta), β-catenin (green) and F-actin (red) (Fig. 4A). First, the area of the cells in μm$^2$ was measured (Fig. 4B). An increase in overall cell area was observed as N-cadherin concentration increased (positive control, 188.0 μm$^2$ ± 29.6 μm$^2$; N-cad 1, 276.0 μm$^2$ ± 45.7 μm$^2$; N-cad 2, 769.0 μm$^2$ ± 41.9 μm$^2$; N-cad 3, 1020.0 μm$^2$ ± 162.0 μm$^2$; and N-cad 5, 1400.0 μm$^2$ ± 345.0 μm$^2$). Cell area on N-cad 3 and N-cad 5 substrates were both significantly larger than the positive control, and on average, 5 times larger. The nuclear area (Fig. 4C), also measured in μm$^2$, followed a similar trend to area and significantly increased with cadherin concentration. However, no difference was found between the positive control (77.6 μm$^2$ ± 27.5 μm$^2$) and the N-cad 1 (83.4 μm$^2$ ± 13.7 μm$^2$) surfaces. The nuclear area of N-cad 2 was 142.0 μm$^2$ ± 9.86 μm$^2$, which was significantly higher than N-cad 1 and the positive control. While no

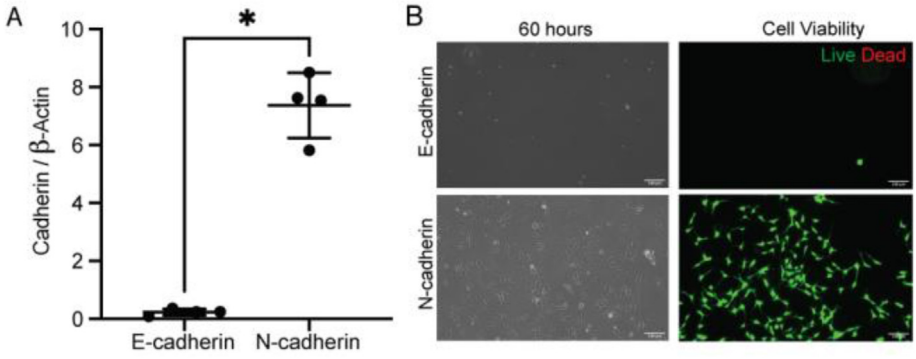


**Fig. 2.** hNSCs express N-cadherin and bind homophilically. A. Significantly more N-cadherin was expressed on cells compared to E-cadherin. Lines indicate mean +/− standard deviation. B. Cell viability of surfaces shown in 2D after 60 h of growth on the surfaces shown phase images and live (green) and dead (red) staining of hNSCs on N and E-cadherin surfaces. No cells adhered to E-cadherin surfaces.

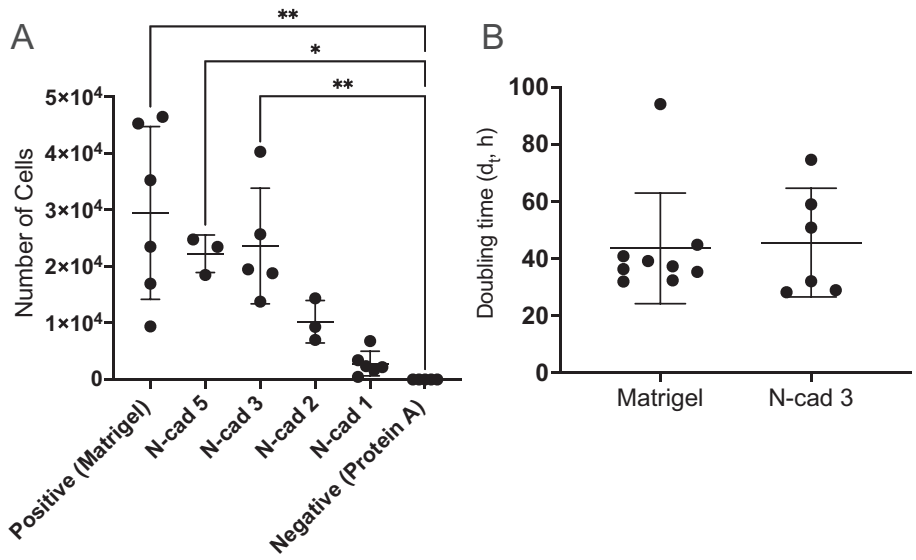


**Fig. 3.** Cells adhered to N-cadherin surfaces. A) Cells equally adhere to positive control (Matrigel®) (n = 6) and N-cad 5 (n = 3) and N-cad 3 (n = 5) N-cadherin substrates. Significant differences were found between the negative control (protein A) (n = 5) and the positive control, N-cad 5, and N-cad 3. N-cadherin substrates N-cad 2 (n = 3) or N-cad 1 (n = 6) did not differ. B) Regardless of the number of cells that adhered for N-Cad 3 or Matrigel, they had the same doubling time.

differences were found between the nucleus area on the two highest cadherin concentrations of N-cad 3 and N-cad 5 (166.0 $\mu m^2 \pm 12.5\ \mu m^2$ and 170.0 $\mu m^2 \pm 2.93\ \mu m^2$ respectively), the average nucleus size of these cells was significantly larger than the two lowest concentration groups. Therefore, the morphology of the cells was further evaluated by counting the number of protrusions. The average number of protrusions (polls) from the cell body increased as cadherin concentration increased, where the control was similar to the low concentration N-cadherin and the three higher concentration groups did not differ per cell (control (1.28 ± 0.141), N-cad 1 (2.05 ± 0.442), N-cad 2 (3.60 ± 00.0367), N-cad 3 (3.37 ± 0.421), and N-cad 5 (3.10 ± 0.489)) (Fig. 4D).

The cells on positive control and low cadherin surfaces did not visually differ in morphology, with cells growing both individually and in small clusters. However, when examining the three higher concentrations of N-cad, cells were significantly larger and many resembled a "fried egg" morphology in phase contrast, with a large nucleus-like yoke and distinct cytoplasmic portion with textured lamellipodia (Fig. S3). Cells on higher concentration surfaces (N-cad 3 and N-cad 5) contained actin stress fibers that appeared as an actin "ring" structure, where stress fibers stretched from the lamellipodia of the cell to a unique ring structure adjacent to, but not surrounding, the nucleus as seen in Fig. 5F. It was observed that the morphology of the fried egg correlated with an actin ring structure once labeled. Due to this unique feature, the percentage of cells that had an actin ring on each substrate was quantified; as cadherin concentration increased, the cells with an actin ring significantly increased. Importantly no actin rings were found on control surfaces (0 % ± 0 %) Most of the cells on lower concentration substrates did not have actin ring formation (N-cad 1, 5.07 % ± 6.00 %; N-cad 2, 40.3 % ± 16.7 %). However, the two higher concentration groups were found to have the majority of cells with an actin ring and the groups did not differ from each other (N-cad 3 (75.5 % ± 7.24 %) and N-cad 5 (70.6 % ± 1.87 %)) (Fig. 5A). The overwhelming majority, >89 % (Fig. S4), of the actin ring structures were found to be adjacent to the nucleus forming a "volcano" like 3D structure (Fig. S5) with the actin stress fibers leading from the lamellipodia to the ring structure at the highest level of the cell. The nucleus was found to stretch throughout the height of the "volcano" structure. As this structure was intriguing, characteristics of the actin ring were further examined to see if the size was responsive to cadherin concentration. The area of the actin ring was found to significantly increased as concentration increased (Fig. 5B); however, no differences were found between the two higher concentration groups.

Next, β-catenin, the portion of the cytosolic catenin protein complex that anchors cadherins within adherens junctions, was examined. β-catenin punctates were characterized by quantifying the number of punctates per cell. As expected, cells on Matrigel had little β-catenin labeling. The cells on N-cad 3 and N-cad 5 substrates had significantly more punctates per cell than those on the positive control (positive control (0.296 ± 0.121), N-cad 1 (1.89 ± 0.905), N-cad 2 (7.81 ± 1.09), N-cad 3 (16.2 ± 2.94), and N-cad 5 (15.0 ± 0.694)) (Fig. 5C). To further characterize the β-catenin labeling, the location of β-catenin within the cell was examined. On cadherin surfaces, β-catenin translocated from diffuse staining in the cytoplasm to defined punctates on the cell perimeter. As cadherin concentration increased, the percentage of cells with β-catenin labeling at the perimeter significantly increased (positive control (5.61 % ± 6.56 %), N-cad 1 (14.9 % ± 13.2 %), N-cad 2 (52.9 % ± 19.5 %), N-cad 3 (92.5 % ± 3.09 %), and N-cad 5 (78.0 % ± 5.22 %)) (Fig. 5D). While examining this labeling, it was noted that β-catenin labeling also colocalized with the unique F-actin ring structure. The percentage of total cells that showed labeling of β-catenin at the actin ring increased with cadherin concentration and was significantly higher in the N-cad 3 than N-cad 1groups (N-cad 1 (6.29 % ± 7.13 %), N-cad 2 (46.6 % ± 8.01 %), N-cad 3 (77.5 % ± 4.46 %), and N-cad 5 (64.8 % ± 7.95 %)) (Fig. 5E).

*Cell mechanotransduction:* YAP translocation is a ubiquitous metric for measuring mechanotransduction.[12,13,25,26] YAP translocation was measured by the ratio of YAP intensity within the nucleus relative to the cytoplasm (Fig. 6A). Translocation was not different on N-cad 1 substrates and control surfaces (1.57 ± 0.26 and 1.82 ± 0.262 respectively). Translocation on N-cad 2 was 2.14 ± 0.095 and was significantly higher than the N-cad 1 groups and significantly less than the translocation of cells on N-cad 3 (2.72 ± 0.216). Interestingly, YAP also colocalized with the actin rings (Fig. 6B). While no differences were found between the control and N-cad 1, the percentage of total cells with YAP at the F-actin ring structure significantly increased for N-cad 2 and N-cad 3 (control (0.0 % ± 0.0 %), N-cad 1 (4.16 ± 3.81), N-cad 2 (26.8 ± 12.4), N-cad 3 (62.2 ± 4.59)). Representative images show nuclei (blue), YAP (green), and F-actin (red) (Fig. 6C).

*Cell differentiation:* Cell fate on N-cadherin surfaces was analyzed via several assessments. Pluripotency, and proliferative activity via SOX2 and Ki67 positive staining, respectively, on control and cadherin surfaces was evaluated after 18–24 h of growth on surfaces. Cells cultured on positive control, N-cad 1 and N-cad 3 were analyzed for the percentage of cells that expressed of SOX2 and Ki67. No differences were found

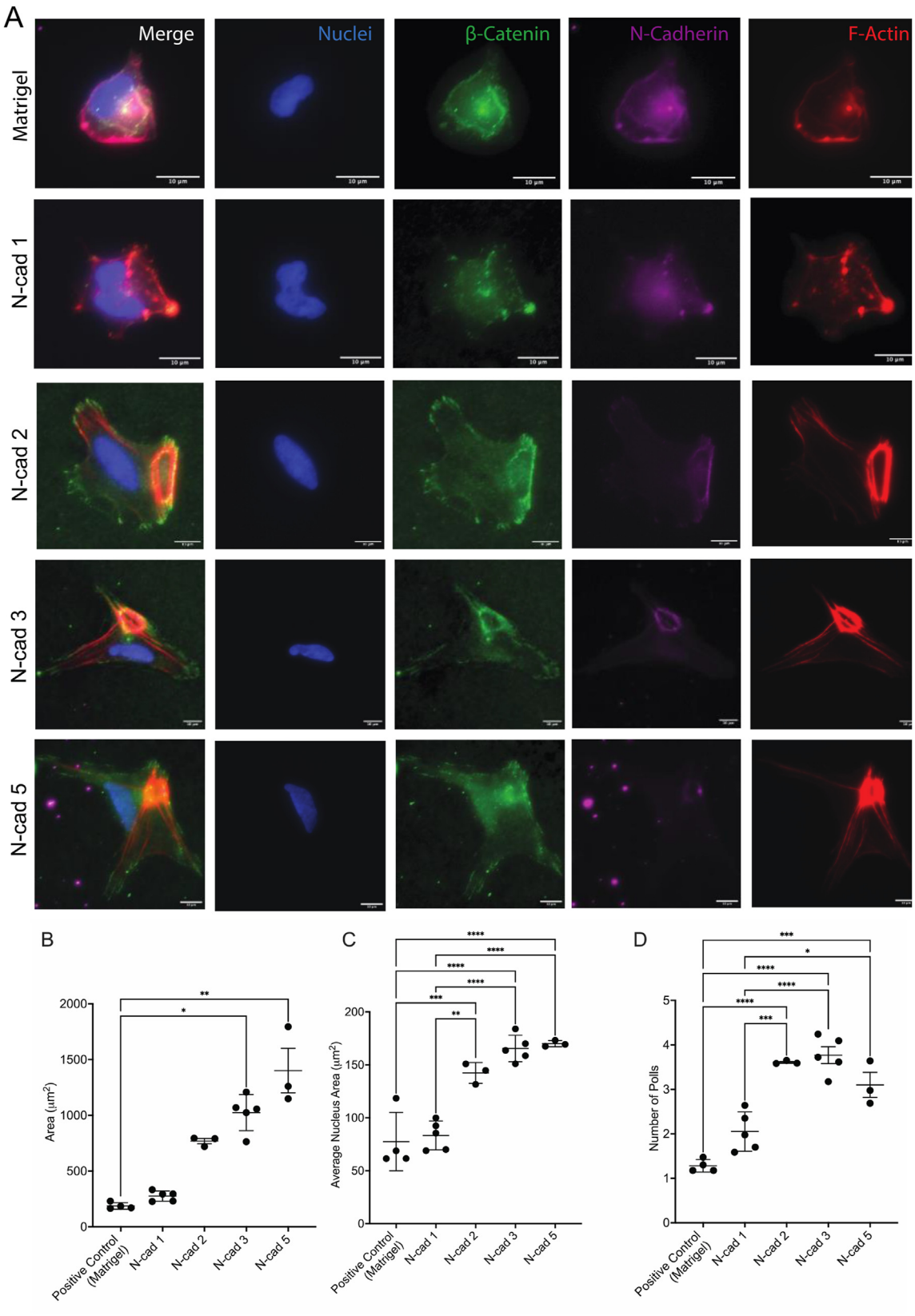


**Fig. 4.** Cell morphology of hNSCs on N-cadherin surfaces is affected by cadherin concentration. A. Representative images of a single cell on the cadherin surface at 63*X*; scale bar is 10 μm in each image. Nuclei (blue), β-catenin (green), N-cadherin (magenta) and F-actin (red). For positive control, N-cad 1, N-cad 2, N-cad 3, and N-cad 5. Scale bar 10 μm. B. Average cell area (μm$^2$). C. Average nucleus area (μm$^2$). D. Average number of cells polls per cell.

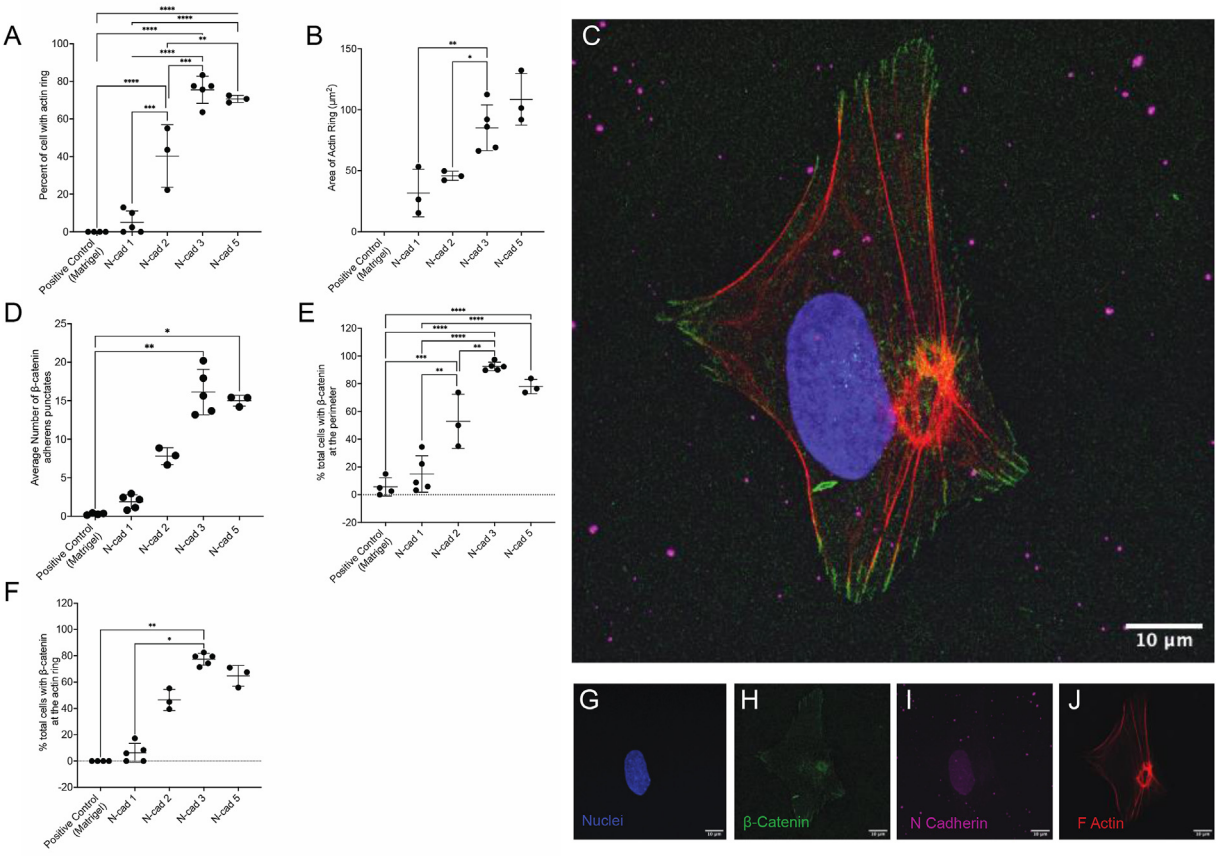


**Fig. 5.** Cadherin concentration alters adherens junction morphology. Actin analysis showed (A) percent of cells with an F-actin ring. (B) Average area of the actin ring. β-catenin analysis showed the (C) average number of adherens points per cell. (D) Location of β-catenin staining showed percentage of cells with β-catenin staining at the edges of the cells. E. Percent of cells with β-catenin staining at the actin ring. All lines represent mean +/− standard deviation. (F) Image taken with a Zeiss LSM 880 with adjusted pinhole of a single cell on the N-cad 3 cadherin surface at 63*X*. (G) Nuclei (blue) (H) β-catenin (green) (I) N-cadherin (magenta) and (J) F-actin (red) are shown separately. Scale bar is 10 μm.

between the surfaces in SOX2 expression (positive control 98.4 % ± 1.91 %, N-cad 1 97.4 % ± 4.20 %, and N-cad 3100.0 % ± 0 %). Percentage of Ki67 positive cells on N-cad 3 (84.1 % ± 3.54 %) was significantly higher compared to positive control (58.4 % ± 14.5 %) but was not different on the N-cad 1 (72.5 % ± 7.52 %) (n = 5) (Fig. S6).

Fig. 6 YAP translocation to the nucleus was analyzed (A) and showed positive control (Matrigel®) (1.82 ± 0.183) and N-cad 1 (1.57 ± 0.262) did not differ. N-cad 2 (2.14 ± 0.0945) was significantly higher than N-cad 1; N-cad 3 showed significantly more translocation compared to all groups (2.72 ± 0.217). (B) The percentage of cells with YAP colocalized with the actin rings, control (0.0 % ± 0.0 %), N-cad 1 (4.16 ± 3.81), N-cad 2 (26.8 ± 12.4), N-cad 3 (62.2 ± 4.59). Lines represent mean +/− standard deviation. (C) Representative images of hNSCs taken at 63*X*, with nuclei (blue), YAP (green) and F-actin (red). Scale bar 10 μm.

However, after 96 h, cells expressing NES via flow cytometry significantly decreased in all N-cad groups compared to Matrigel® controls (97.9 % ± 1.63 % (control), 87.9 % ± 2.71 % (N-cad 1), 91.2 % ± 1.75 % (N-cad 2), and 91.1 % ± 0.911 % (N-cad 3)) (Fig. 7B). Neither GFAP (69.2 % ± 4.38 % (control), 66.0 % ± 8.43 % (N-cad 1), 71.0 % ± 8.39 % (N-cad 2), and 56.7 % ± 0.547 % (N-cad 3)) (Fig. 7A) nor S100β (0.003 % ± 0.005 % (control), 0.023 % ± 0.023 % (N-cad 1), 0.050 % ± 0.036 % (N-cad 2), and 0.030 % ± 0.030 % (N-cad 3)) (Fig. 7C) differed based on culture surface. However, significantly fewer β-III tubulin expressing cells were found on Matrigel® compared to N-cad 3 (28.7 % ± 10.1 % (control), 49.1 % ± 11.1 % (N-cad 1), 47.0 % ± 6.13 % (N-cad 2), and 59.8 % ± 7.58 % (N-cad 3)) (Fig. 7D). Immunocytochemistry was used to confirm flow cytometry, labeling nuclei, nestin, β-III tubulin and S100β. Neuron-like extensions can be seen in the cadherin samples (Fig. 7E).

## 4. Discussion

Pluripotent NSCs reside in a cell dense zone in the SVZ; they receive signals from the microenvironment to determine their fate. In the dense microenvironment, cell:cell mechanotransduction would occur between adjacent cells via cadherin molecules. Therefore, the goal of this work was to examine if cadherin interactions between hiPSC-derived NSC and N-cadherin substrates induced mechanotransduction. As lateral clustering of cadherins in native cell–cell contact points is a vital part of junctional maturation and mechanotransduction, we first characterized the substrate and number of cadherins available. The tethered surfaces in this study were initially made with Protein A as it binds to up to 5 human immunoglobulin Fc to create opportunities for clustering of cadherins as the relative amount of cadherin increased. However, we found that for each of our substrates, the amount of cadherin per surface was only a small portion of the cadherin that was applied, ranging from $8 \times 10^8$ to $4 \times 10^9$ bound molecules per $cm^2$. These numbers are similar in magnitude to the range of molecules per area for clustering proteins such as integrins, cadherins, and major histocompatibility complexes,[27] suggesting that our substrates were in the correct range to study clustering interactions. The increase in available and, essentially, "pre-clustered" cadherin, while difficult to quantify, could increase the probability of adherens-like junction formation and mechanotransduction. Therefore, we moved forward with these substrates to examine cadherin interactions with hNSCs.

Initial examination of the expression of NES, SOX2, and GFAP on hNSCs used in the current study indicated that the cells were similar to multipotent neural stem cells (type B) found in the subventricular zone.[28] As E-cadherin has also been found to play an important component of the

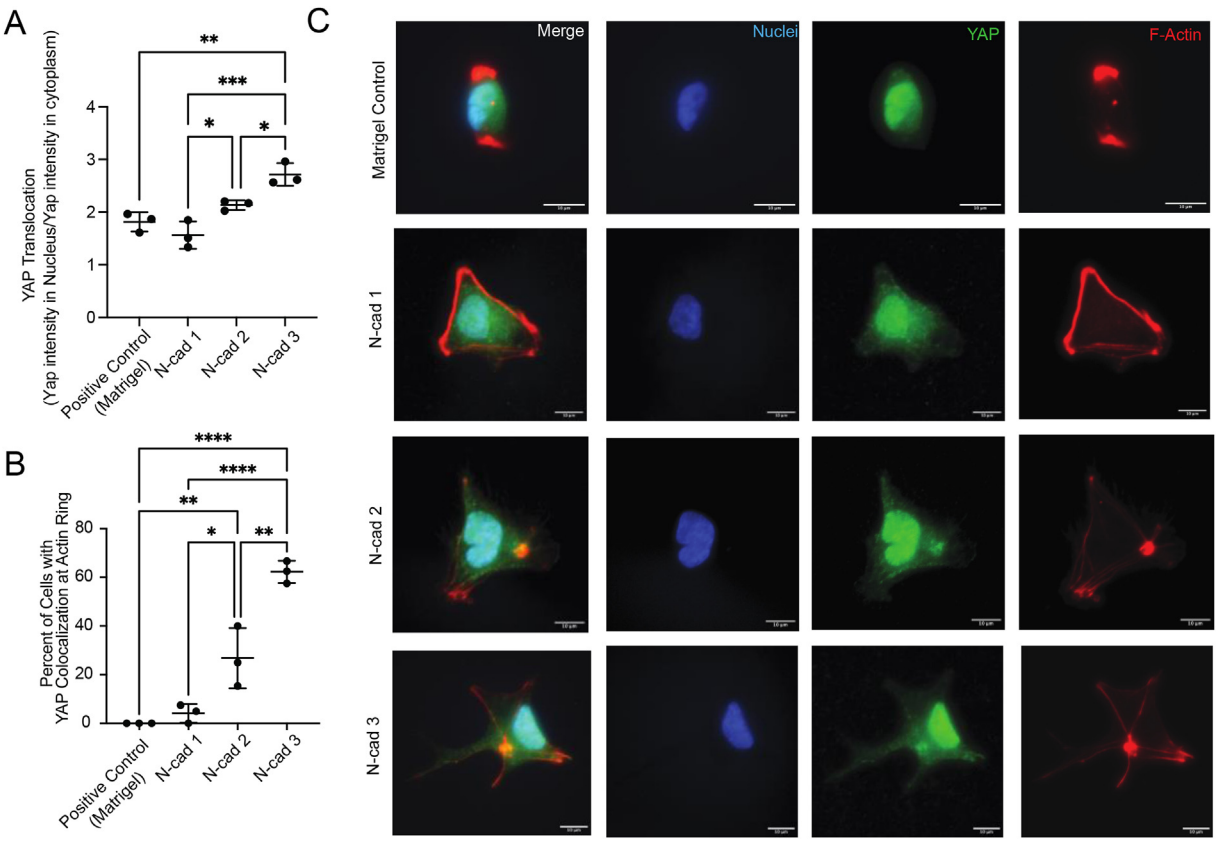


**Fig. 6.** YAP translocation to the nucleus was analyzed (A) and showed positive control (Matrigel®) (1.82 ± 0.183) and N-cad 1(1.57 ± 0.262) did not differ. N-cad 2 (2.14 ± 0.0945) was significantly higher than N-cad 1; N-cad 3 showed significantly more translocation compared to all groups (2.72 ± 0.217). (B) The percentage of cells with YAP colocalized with the actin rings, control (0.0% ± 0.0%), N-cad 1 (4.16 ± 3.81), N-cad 2 (26.8 ± 12.4), N-cad 3 (62.2 ± 4.59). Lines represent mean +/- standard deviation. (C) Representative images of hNSCs taken at 63X, with nuclei (blue), YAP (green) and F-actin (red). Scale bar 10 μm.

NSC niche,[29] the iPSC-derived NSCs were examined for both E- and N-cadherin. Baseline assessment of hNSC protein expression showed that cells expressed N-cadherin, but not E-cadherin. However, previous studies have demonstrated that cells can use cadherins to bind heterophilically.[8] Therefore, we examined if the cells would bind to E-cadherin substrates. However, we found that these cells bound only homophilically to tethered N-cadherin. As there were not any viable cells on E-cadherin substrates, we continued the studies with N-cadherin substrates only.

Morphology is often used as an initial assessment of the mechanotransductive relationship between cells and their environment.[30–32] In previous studies, both size and shape were used to indicate interaction with cadherin, junctional maturation, and subsequent mechanosensing activity.[30] Here, both cell and nuclear area increased with increasing N-cadherin concentration on the substrate. However, we found that the average increase in nuclear area decreased relative to the average area of the cells (Fig. S7), a ratio that is highly regulated in terminal cells.[33] Previous work has noted that stem cells have higher nuclear:cell volumetric ratios than differentiated or aged cells,[34,35] similar to what we are seeing here within 24 h for area ratio. Nuclei in stem cells have also been found to have increased deformability compared to differentiated cells,[36,37] which may lead to an increased ability to be affected by cytoskeletal reorganization and strong binding interactions. Overall, increases in cell and nuclear size are energy intensive as the cell must deviate energy from normal functions; the biological "cost" of performing expansion instead of other vital functions led us to investigate what other morphological changes were occurring.

In addition to overall size, cells increased lamellipodial-like protrusions and F-actin structure formation as cadherin concentration increased. These structures were similar to those found by Gavard et al. in which a "fried egg" shape of cells was characterized in both mouse myogenic and S18 chick cells grown on 5–10 μg/cm$^2$ of applied, adsorbed N-cadherin.[38] In our work, the lamellipodia were found to be rich in F-actin and β-catenin (Fig. 5). While stress fiber accumulation or polarization of cells has been observed in previous studies,[13,38,39] the distinct "ring" structure of F-actin that was adjacent to the nucleus has not previously been reported in single hNSCs to our knowledge. Geometric formations of F-actin have been noted in multicellular clusters, including in neural rosettes,[40] in a podosome belt[41] and in cross-linked actin networks in ocular meshwork.[42] In single cells, however, actin rings are often on the cell cortex around the nucleus forming contractile rings during mitosis or concentrated in the lamellipodia during cell migration.[43] To the best of our knowledge, this work is the first documentation of cells forming a ring-shaped actomyosin architecture adjacent to the nucleus. The formation of these actin structures implied that the cells are sensing the interactions with N-cadherin as interactions with other cells, therefore we then investigated whether these novel actin structures were indicative of mechanotransduction.

YAP translocation has been utilized to demonstrate mechanosensitive interactions between cells and their surrounding environment, including between N-cadherin mimics and mesenchymal stem cells.[13,25,39] Here we have shown YAP translocation to the nucleus increased with increased concentration N-cadherin substrates. Previous work has demonstrated that YAP nuclear localization was dependent upon amount of F-actin.[44] F-actin cytoskeletal ring structures formed with increasing N-cadherin concentration that altered cell morphology and increased β-catenin punctates at the edges of cells, indicating increased tension environments. While adherens junction formation has been found to sustain YAP-phosphorylation,[45] high tension at these junctions also can inhibit the phosphorylation and support translocation to the nucleus.[46,47] In this

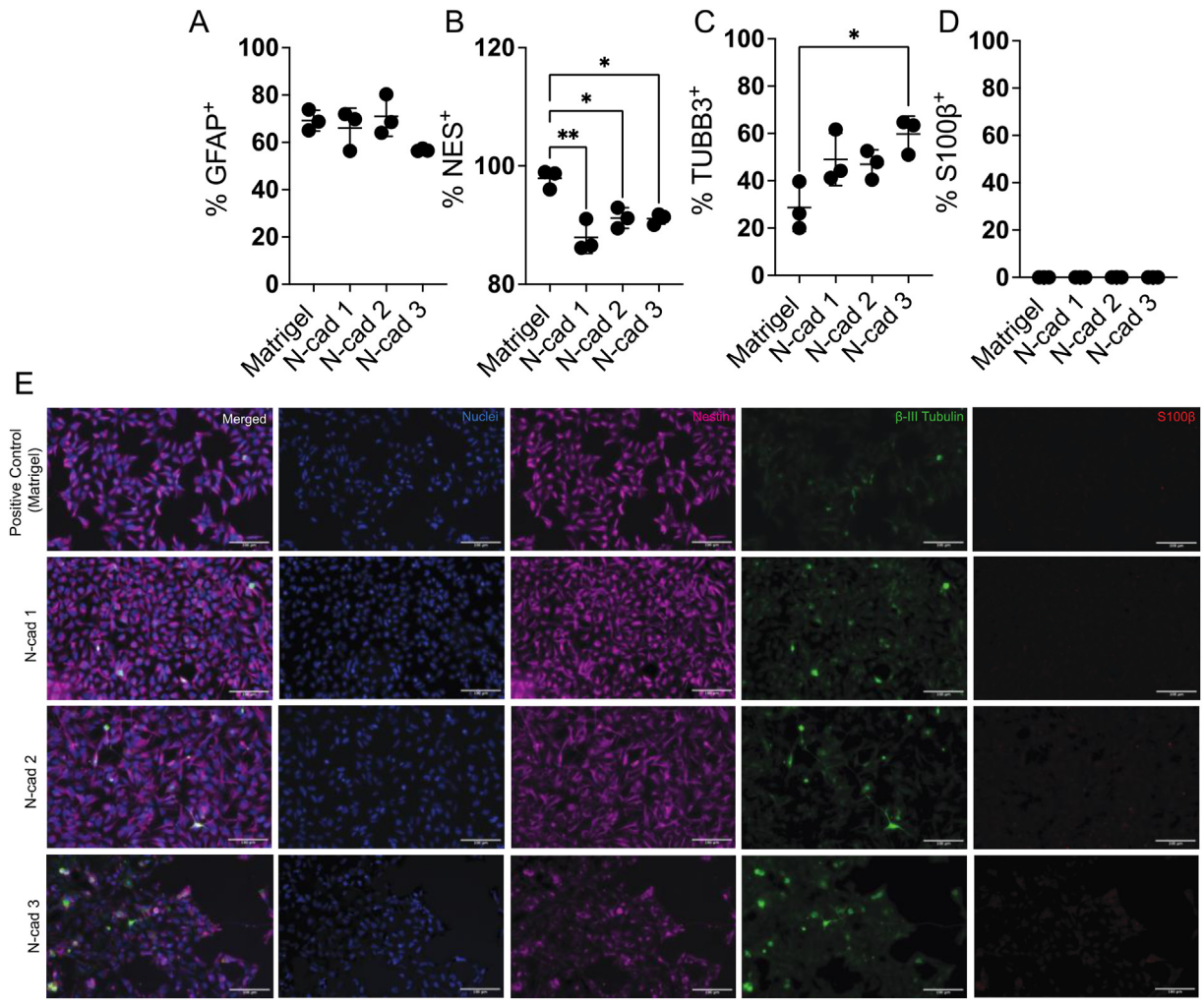


**Fig. 7.** Cells differentiated towards neurons on cadherin surfaces. A-D. Flow cytometry shows percent of cells on Matrigel and N-cadherin surfaces expressing (A) GFAP (B) nestin (C) β-III tubulin, and (D) S100β, and we found significantly less β-III tubulin expressing cells on Matrigel compared to N-cadherin, n = 3. (E) Immunohistochemistry of hNSCs on control and N-cadherin; nuclei (blue), nestin (magenta), β-III tubulin (green) and S100β (red) taken at 20*X*, scale bar 100 μm.

study, YAP was localized to the F-actin structures that increased with increased surface N-cadherin. As YAP has been found to bind with angiomotin, anchoring YAP to F-actin stress fibers, these F-actin structures could retain YAP in the cytoplasm, and make it unable translocate to the nucleus.[25,48,49] Even with this cytoplasmic sequestration, overall YAP translocation indicated that exogenous N-cadherin elicited mechanosensing events relative to the amount of cadherin.

In addition to YAP localization to the F-actin structures, we also saw β-catenin localization to these structures and decided to investigate further. As is typical with N-cadherin binding, we found that β-catenin punctate formation at the cell membrane increased with cadherin concentration. The location of β-catenin staining was important to identify as it can act as a transcription factor within the nucleus when not phosphorylated at the cell membrane.[6,50] Therefore, localization of β-catenin at both the cell membrane and within the F-actin ring indicated sequestration of β-catenin in the cytoplasm. Concentration and localization of β-catenin has previously been implicated in mouse ESC self-renewal and differentiation, depending on the dose and conditions,[51] and apoptosis or neurogenesis in neural stem cells, depending on the dynamics and regulation of β-catenin.[52,53] Therefore, we next sought to investigate the resulting impact of culture on N-cadherin substrates on NSC maintenance.

YAP translocation to the nucleus and sequestration at the actin ring along with the localization of β-catenin at the cell membrane provide signals of both proliferation and differentiation to the cells. Within the first 24 h after seeding, cells remain proliferative and pluripotent on all substrates. After 96 h on N-cadherin surfaces, hNSCs express significantly less nestin, with a corresponding increase in the percentage of cells expressing the neuronal marker β-III tubulin, particularly on higher N-cadherin concentrations. N-cadherin expression levels have been shown to play a role in differentiation of other stem cell types, including muscle cell differentiation[54] and differentiation of MSCs.[13] A recent study showed that following neurulation in a mouse model, E-cadherin promoted pluripotency[55] and an increase in N-cadherin expression correlated with NSCs leaving the niche toward stable neurogenesis both *in vivo* and *in vitro*.[56] While there are differences between the rodent and human SVZ,[57] radial glial-like stem cells are found similarly in both models. With no exogenous soluble factors, high cadherin substrates (N-cad 3) drove hNSCs to differentiation neuronally over a time span of 4 days. Differentiation over such a short time frame may be attributed the extensive cytoskeletal reorganization and subsequent localization of transcription factors YAP and β-catenin in response to cadherin in a concentration dependent manner. The findings presented show the potential of N-cadherin to induce neurogenic differentiation of pluripotent hNSCs in a short timeframe without other additives.

## 5. Conclusion

In summary, tethered, recombinant cadherin surfaces were fabricated with different amounts of N-cadherin. Homophilic binding between

hNSCs and exogenous cadherin was found to be dependent upon the amount of cadherin applied and may be indicative of clustering ability and junctional maturation. Increases in the amount of cadherin on the substrates led to a proportional increase in cell and nuclear area that was accompanied by increase in unique F-actin ring rearrangement and adherens junctional formation. YAP translocation to the nucleus and sequestration in the actin-rings indicated mechanotransduction was occurring and analysis of differentiation state showed that cells on the surfaces with increased cadherin available were undergoing neuronal differentiation. The role of N-cadherin and the effect of incorporating different amounts of N-cadherin on the potential for perturbing the gene expression via mechanotransductive events in a short timeframe was highlighted. We show that relative amount of cadherin used is important and can have direct impacts on *in vitro* outcomes and is not clearly documented in many of the reports cited. The results have implications in the role of N-cadherin in design of biomaterials to mimic the neurogenic niche.

## CRediT authorship contribution statement

**McKay Cavanaugh:** Writing – original draft, Visualization, Validation, Methodology, Investigation, Formal analysis, Data curation. **Rebecca Kuntz Willits:** Writing – review & editing, Visualization, Validation, Supervision, Resources, Project administration, Methodology, Investigation, Funding acquisition, Conceptualization.

## Ethics

This study does not contain any studies with human or animal subjects performed by any of the authors.

## Notes

The authors declare no competing financial interests.

## Funding sources

This work was supported by the National Science Foundation (2113403) and the Alsaif Fellowship from Northeastern University for partial funding support for MMC.

## Declaration of competing interest

The authors declare the following financial interests/personal relationships which may be considered as potential competing interests: Rebecca Willits reports financial support was provided by National Science Foundation. If there are other authors, they declare that they have no known competing financial interests or personal relationships that could have appeared to influence the work reported in this paper.

## Acknowledgment

The authors would like to thank Professor Sanjeev Mukerjee of the Northeastern University Center for Renewable Energy Technology for use of the FTIR machine. We thank the Institute for Chemical Imaging of Living Systems (RRID:SCR_022681) at Northeastern University for consultation and instrument support for use of the Zeiss LSM 880. XPS was performed at the Harvard University Center for Nanoscale Systems (CNS); a member of the National Nanotechnology Coordinated Infrastructure Network (NNCI), which is supported by the National Science Foundation under NSF award no. ECCS-2025158. We acknowledge Alexia Angulo and Marisa Parker for their assistance. Last, we acknowledge Dr. Ge Zhang, Dr. Denise Inman, Dr. Rouzbeh Amini, Dr. Harikrishnan Parameswaran, and Dr. Narges Yazdani for helpful discussion of the results.

## Appendix A. Supplementary data

Supplementary data to this article can be found online at https://doi.org/10.1016/j.mbm.2024.100099.

## References

1. Takagi Y. History of neural stem cell research and its clinical application. *Neurol Med -Chir*. 2016;56(3):110–124. https://doi.org/10.2176/nmc.ra.2015-0340.
2. Ioannidis K, Angelopoulos I, Gakis G, et al. 3D reconstitution of the neural stem cell niche: connecting the dots. *Front Bioeng Biotechnol*. 2021;9:705470. https://doi.org/10.3389/fbioe.2021.705470.
3. Altman J, Das G. Postnatal neurogenesis in the Guinea-pig. *Nature*. 1967;214:1098–1101. https://doi.org/10.1038/2141098a0.
4. Ratheesh A, Yap AS. A bigger picture: classical cadherins and the dynamic actin cytoskeleton. *Nat Rev Mol Cell Biol*. 2012;13(10):673–679. https://doi.org/10.1038/nrm3431.
5. Schwartz MA, DeSimone DW. Cell adhesion receptors in mechanotransduction. *Curr Opin Cell Biol*. 2008;20(5):551–556. https://doi.org/10.1016/j.ceb.2008.05.005.
6. Leckband DE, de Rooij J. Cadherin adhesion and mechanotransduction. *Annu Rev Cell Dev Biol*. 2014;30:291–315. https://doi.org/10.1146/annurev-cellbio-100913-013212.
7. Perez TD, Nelson WJ. Cadherin adhesion: mechanisms and molecular interactions. *Handb Exp Pharmacol*. 2004;165:3–21. https://doi.org/10.1007/978-3-540-68170-0_1.
8. Tabdili H, Langer M, Shi Q, Poh YC, Wang N, Leckband D. Cadherin-dependent mechanotransduction depends on ligand identity but not affinity. *J Cell Sci*. 2012;125(Pt 18):4362–4371. https://doi.org/10.1242/jcs.105775.
9. Braga V. Cell–cell adhesion and signalling. *Curr Opin Cell Biol*. 2002;14(5):546–556. https://doi.org/10.1016/s0955-0674(02)00373-3.
10. Venhuizen JH, Jacobs FJC, Span PN, Zegers MM. P120 and E-cadherin: double-edged swords in tumor metastasis. *Semin Cancer Biol*. 2020;60:107–120. https://doi.org/10.1016/j.semcancer.2019.07.020.
11. Di-Luoffo M, Ben-Meriem Z, Lefebvre P, Delarue M, Guillermet-Guibert J. PI3K functions as a hub in mechanotransduction. *Trends Biochem Sci*. 2021;46(11):878–888. https://doi.org/10.1016/j.tibs.2021.05.005.
12. Elosegui-Artola A, Andreu I, Beedle AEM, et al. Force triggers YAP nuclear entry by regulating transport across nuclear pores. *Cell*. 2017;171(6):1397–1410. https://doi.org/10.1016/j.cell.2017.10.008.
13. Qin EC, Ahmed ST, Sehgal P, Vu VH, Kong H, Leckband DE. Comparative effects of N-cadherin protein and peptide fragments on mesenchymal stem cell mechanotransduction and paracrine function. *Biomaterials*. 2020;239:119846. https://doi.org/10.1016/j.biomaterials.2020.119846.
14. Tian W, Yu J, Tomchick DR, Pan D, Luo X. Structural and functional analysis of the YAP-binding domain of human TEAD2. *Proc Natl Acad Sci U S A*. 2010;107(16):7293–7298. https://doi.org/10.1073/pnas.1000293107.
15. Zhang J, Shemezis JR, McQuinn ER, Wang J, Sverdlov M, Chenn A. AKT activation by N-cadherin regulates beta-catenin signaling and neuronal differentiation during cortical development. *Neural Dev*. 2013;8:7. https://doi.org/10.1186/1749-8104-8-7.
16. Yagita Y, Sakurai T, Tanaka H, Kitagawa K, Colman DR, Shan W. N-cadherin mediates interaction between precursor cells in the subventricular zone and regulates further differentiation. *J Neurosci Res*. 2009;87(15):3331–3342. https://doi.org/10.1002/jnr.22044.
17. Erickson HP. Size and shape of protein molecules at the nanometer level determined by sedimentation, gel filtration, and electron microscopy. *Biol Proced Online*. 2009;11:32–51. https://doi.org/10.1007/s12575-009-9008-x.
18. Jassim AH, Cavanaugh M, Shah JS, Willits R, Inman DM. Transcorneal electrical stimulation reduces neurodegenerative process in a mouse model of glaucoma. *Ann Biomed Eng*. 2021;49(2):858–870. https://doi.org/10.1007/s10439-020-02608-8.
19. Schindelin J, Arganda-Carreras I, Frise E, et al. Fiji: an open-source platform for biological-image analysis. *Nat Methods*. 2012;9(7):676–682. https://doi.org/10.1038/nmeth.2019.
20. Gonzalez-Perez O, Quiñones-Hinojosa A. Astrocytes as neural stem cells in the adult brain. *J Stem Cell*. 2012;7(3):181–188.
21. Roskams AJI, Cai X, Ronnett GV. Expression of neuron-specific beta-III tubulin during olfactory neurogenesis in the embryonic and adult rat. *Neuroscience*. 1998;83(1):191–200. https://doi.org/10.1016/S0306-4522(97)00344-8.
22. Raponi E, Agenes F, Delphin C, et al. S100B expression defines a state in which GFAP-expressing cells lose their neural stem cell potential and acquire a more mature developmental stage. *Glia*. 2007;55(2):165–177. https://doi.org/10.1002/glia.20445.
23. Duvault Y, Gagnaire A, Gardies F, et al. Physicochemical characterization of covalently bonded alkyl monolayers on silica surfaces. *Thin Solid Films*. 1990;185(1):169–179. https://doi.org/10.1016/0040-6090(90)90016-7.
24. Gallant ND, Lavery KA, Amis EJ, Becker ML. Universal gradient substrates for “Click” biofunctionalization. *Adv Mater*. 2007;19(7):965–969. https://doi.org/10.1002/adma.200602221.
25. Dupont S, Morsut L, Aragona M, et al. Role of YAP/TAZ in mechanotransduction. *Nature*. 2011;474(7350):179–183. https://doi.org/10.1038/nature10137.
26. Matsui Y, Lai Z-C. Mutual regulation between Hippo signaling and actin cytoskeleton. *Protein & Cell*. 2013;4(12):904–910. https://doi.org/10.1007/s13238-013-3084-z.

27. Changede R, Sheetz M. Integrin and cadherin clusters: a robust way to organize adhesions for cell mechanics. *Bioessays*. 2017;39(1):1–12. https://doi.org/10.1002/bies.201600123.
28. Alvarez-Palazuelos LE, Robles-Cervantes MS, Castillo-Velazquez G, et al. Regulation of neural stem cell in the human SVZ by trophic and morphogenic factors. *Curr Signal Transduct Ther*. 2011;6(3):320–326. https://doi.org/10.2174/157436211797483958.
29. Karpowicz P, Willaime-Morawek S, Balenci L, DeVeale B, Inoue T, van der Kooy D. E-cadherin regulates neural stem cell self-renewal. *J Neurosci*. 2009;29(12):3885. https://doi.org/10.1523/JNEUROSCI.0037-09.2009.
30. Wolfenson H, Yang B, Sheetz MP. Steps in mechanotransduction pathways that control cell morphology. *Annu Rev Physiol*. 2019;81:585–605. https://doi.org/10.1146/annurev-physiol-021317-121245.
31. Benham-Pyle Bp B, Nelson W. Mechanical strain induces E-cadherin–dependent Yap 1 and β-catenin activation to drive cell cycle entry. *Science*. 2015;348(6238):1024–1027.
32. Zaidel-Bar R. Cadherin adhesome at a glance. *J Cell Sci*. 2013;126(Pt 2):373–378. https://doi.org/10.1242/jcs.111559.
33. Mukherjee RN, Chen P, Levy DL. Recent advances in understanding nuclear size and shape. *Nucleus*. 2016;7(2):167–186. https://doi.org/10.1080/19491034.2016.1162933.
34. McColloch A, Rabiei M, Rabbani P, Bowling A, Cho M. Correlation between nuclear morphology and adipogenic differentiation: application of a combined experimental and computational modeling approach. *Sci Rep*. 2019;9(1):16381. https://doi.org/10.1038/s41598-019-52926-8.
35. Lengefeld J, Cheng C-W, Maretich P, et al. Cell size is a determinant of stem cell potential during aging. Sci Adv. 7(46):eabk0271.doi:10.1126/sciadv.abk0271.
36. Pajerowski JD, Dahl KN, Zhong FL, Sammak PJ, Discher DE. Physical plasticity of the nucleus in stem cell differentiation. *Proc Natl Acad Sci U S A*. 2007;104(40):15619–15624. https://doi.org/10.1073/pnas.0702576104.
37. Heo S-J, Driscoll TP, Thorpe SD, et al. Differentiation alters stem cell nuclear architecture, mechanics, and mechano-sensitivity. *Elife*. 2016;5:e18207. https://doi.org/10.7554/eLife.18207.
38. Gavard J, Lambert M, Grosheva I, et al. Lamellipodium extension and cadherin adhesion: two cell responses to cadherin activation relying on distinct signalling pathways. *J Cell Sci*. 2004;117(Pt 2):257–270. https://doi.org/10.1242/jcs.00857.
39. Cosgrove BD, Mui KL, Driscoll TP, et al. N-cadherin adhesive interactions modulate matrix mechanosensing and fate commitment of mesenchymal stem cells. *Nat Mater*. 2016;15(12):1297–1306. https://doi.org/10.1038/nmat4725.
40. Wilson PG, Stice SS. Development and differentiation of neural rosettes derived from human embryonic stem cells. *Stem Cell Rev*. 2006;2(1):67–77. https://doi.org/10.1007/s12015-006-0011-1.
41. Burgess Y-xQ Teresa L, Kaufman Stephen, Ring Brian D, et al. The ligand for osteoprotegerin (OPGL) directly activates mature osteoclasts. *JCB (J Cell Biol)*. 1999;145:527–538. https://doi.org/10.1083/jcb.145.3.527.
42. Bermudez JY, Montecchi-Palmer M, Mao W, Clark AF. Cross-linked actin networks (CLANs) in glaucoma. *Exp Eye Res*. 2017;159:16–22. https://doi.org/10.1016/j.exer.2017.02.010.
43. Cronin NM, DeMali KA. Dynamics of the actin cytoskeleton at adhesion complexes. *Biology*. 2021;11(1). https://doi.org/10.3390/biology11010052.
44. Das A, Fischer RS, Pan D, Waterman CM. YAP nuclear localization in the absence of cell-cell contact is mediated by a filamentous actin-dependent, myosin II- and phospho-YAP-independent pathway during extracellular matrix mechanosensing. *J Biol Chem*. 2016;291(12):6096–6110. https://doi.org/10.1074/jbc.M115.708313.
45. Karaman R, Halder G. Cell junctions in hippo signaling. *Cold Spring Harb Perspect Biol*. 2018;10(5). https://doi.org/10.1101/cshperspect.a028753.
46. Campas O, Noordstra I, Yap AS. Adherens junctions as molecular regulators of emergent tissue mechanics. *Nat Rev Mol Cell Biol*. 2024;25(4):252–269. https://doi.org/10.1038/s41580-023-00688-7.
47. Rauskolb C, Sun S, Sun G, Pan Y, Irvine KD. Cytoskeletal tension inhibits Hippo signaling through an Ajuba-Warts complex. *Cell*. 2014;158(1):143–156. https://doi.org/10.1016/j.cell.2014.05.035.
48. Zaltsman Y, Masuko S, Bensen JJ, Kiessling LL. Angiomotin regulates YAP localization during neural differentiation of human pluripotent stem cells. *Stem Cell Rep*. 2019;12(5):869–877. https://doi.org/10.1016/j.stemcr.2019.03.009.
49. Kang PH, Schaffer DV, Kumar S. Angiomotin links ROCK and YAP signaling in mechanosensitive differentiation of neural stem cells. *Mol Biol Cell*. 2020;31(5):386–396. https://doi.org/10.1091/mbc.E19-11-0602.
50. Wisniewska MB. Physiological role of beta-catenin/TCF signaling in neurons of the adult brain. *Neurochem Res*. 2013;38(6):1144–1155. https://doi.org/10.1007/s11064-013-0980-9.
51. Kim H, Wu J, Ye S, et al. Modulation of β-catenin function maintains mouse epiblast stem cell and human embryonic stem cell self-renewal. *Nat Commun*. 2013;4:2403. https://doi.org/10.1038/ncomms3403.
52. Gao J, Liao Y, Qiu M, Shen W. Wnt/β-Catenin signaling in neural stem cell homeostasis and neurological diseases. *Neurosci*. 2020;27(1):58–72. https://doi.org/10.1177/1073858420914509.
53. Rosenbloom AB, Tarczyński M, Lam N, Kane RS, Bugaj LJ, Schaffer DV. β-Catenin signaling dynamics regulate cell fate in differentiating neural stem cells. *Proc Natl Acad Sci USA*. 2020;117(46):28828–28837. https://doi.org/10.1073/pnas.2008509117.
54. Goel AJ, Rieder MK, Arnold HH, Radice GL, Krauss RS. Niche cadherins control the quiescence-to-activation transition in muscle stem cells. *Cell Rep*. 2017;21(8):2236–2250. https://doi.org/10.1016/j.celrep.2017.10.102.
55. Malaguti M, Nistor PA, Blin G, Pegg A, Zhou X, Lowell S. Bone morphogenic protein signalling suppresses differentiation of pluripotent cells by maintaining expression of E-Cadherin. *Elife*. 2013;2:e01197. https://doi.org/10.7554/eLife.01197.
56. Punovuori K, Migueles RP, Malaguti M, et al. N-cadherin stabilises neural identity by dampening anti-neural signals. *Development*. 2019;146(21):dev183269. https://doi.org/10.1242/dev.183269.
57. Tabata H, Yoshinaga S, Nakajima K. Cytoarchitecture of mouse and human subventricular zone in developing cerebral neocortex. *Exp Brain Res*. 2012;216(2):161–168. https://doi.org/10.1007/s00221-011-2933-3.